PROCEEDINGS, 47th Workshop on Geothermal Reservoir Engineering
Stanford University, Stanford, California, February 7-9, 2022
SGP-TR-223

# The Use of Reversibly Adsorbing Tracers for Characterizing Unconventional-Petroleum Reservoirs at Geothermal-Reservoir Temperatures

Peter E. Rose[1], Michael Mella[1] and Mark Williams[2]

[1]Energy & Geoscience Institute at the University of Utah, 423 Wakara Way suite 300, Salt Lake City, Utah 84108

prose@egi.utah.edu

[2]INTERA Geoscience and Engineering Solutions

**Keywords:** geothermal energy, shale-oil, shale-gas, unconventional petroleum, polyaromatic sulfonates, solute tracers

## ABSTRACT

We conducted a series of laboratory and field tests in order to characterize flow processes during the hydrofracture and production of a Horn River, Canada shale-gas reservoir. The heat from this unconventional-petroleum reservoir was not co-produced with the petroleum, but, if it were, this system, with down-hole measured temperatures of 140 °C, could qualify as a low-temperature geothermal reservoir. Laboratory studies were conducted using a bench-top flow reactor in which we simulated reservoir conditions using drill cuttings from shale formations. In the subsequent field experiment, we injected a combination of conservative and reactive tracers into each of 10 long-reach horizontal wells. Water samples were collected during the flowback portion of the test from each of the wells and the concentrations of the conservative and reversibly adsorbing tracers were measured at EGI. In most cases, within each formation, the gas production rate was proportional to the relative degree of adsorption of the reversibly adsorbing tracer. Using the laboratory-obtained tracer-rock interaction data, a numerical simulation model of the injection/flowback process was built. The model was then used to calculate tracer-contacted fracture-surface area adjacent to each well, which was used to correlate with gas production rate.

## 1. INTRODUCTION

Chemical tracing in geothermal and unconventional-petroleum settings involves the tracking of fluids through subterranean reservoirs using tracers that are typically injected through injection wells and produced at production wells or springs, where their concentrations are measured. The flow is often between wells, but can occasionally involve injection and backflow through a single well, as is typical of unconventional (shale-oil and shale-gas) petroleum systems.

Tracers can be characterized as belonging to either of two broad categories—conservative or reactive. Conservative tracers are those that interact neither with the reservoir rock nor with the solvent as they are advected through the formation; their flow is therefore effectively indistinguishable from that of the solvent molecules. Measured conservative-tracer concentrations and tracer-arrival times can serve to interpret interwell flow patterns, pore volumes, and reservoir dispersivity (Rose et al., 2004; Shook et al., 2005).

In addition to possessing good thermal stability, solute tracers must also be very detectable, environmentally benign, nontoxic, available in bulk and affordable. One family of compounds that meets these requirements and that has been used extensively in geothermal reservoirs around the globe is the naphthalene sulfonates (Figure 1). They possess excellent detectability by High Performance Liquid Chromatography-fluorescence, since the polyaromatic backbone provides a large cross-section for absorption for subsequent fluorescent emission. A low detection limit in turn means that lower quantities are required for fullscale applications. These compounds are nontoxic, environmentally benign (Greim et al., 1994) and available in bulk.

The naphthalene sulfonates have been shown to exhibit excellent resistance to thermal degradation in laboratory studies under conditions that simulate the reducing environment of a geothermal field (Rose et al., 2001). These laboratory results have been confirmed in numerous field tests (Rose et al., 2002a; Rose et al. 2002b; Rose et al., 2003). However, in a series of laboratory experiments that exposed the naphthalene sulfonate tracers to mineral surfaces and temperatures found in some of the world's hottest (>300°C) geothermal reservoirs, they were shown to isomerize and/or degrade—especially when exposed to these high temperatures for long residence times (Sajkowski, L., 2020).

Due to their successful use in hundreds of geothermal tracer tests around the world, the naphthalene sulfonates have been used in hot, unconventional (shale-oil and shale-gas) petroleum applications, where reservoir temperatures can approach 200 °C and conventional (halogenated benzoate) petroleum tracers fail, e.g., Horn River, Austin Chalk, Eagle Ford, and Permian Basin shales. In side-by-side tests between the naphthalene sulfonates and the halogenated benzoates in laboratory flow experiments under simulated reservoir conditions, using drill cuttings from a variety of shale reservoirs, the latter tracers were either thermally degraded or adsorbed to rock surfaces and therefore produced at only a few percent of a co-injected chloride control, whereas the naphthalene sulfonates showed no diminution in concentration relative to a chloride control. These laboratory observations were confirmed in field studies in shale-gas (Horn River and Austin Chalk) reservoir settings (unpublished).

| Compound | Structure | Excitation / Emission (nm) |
|---|---|---|
| *1-naphthalene sulfonate* |  | *217 / 333* |
| *2-naphthalene sulfonate* |  | *220 / 336* |
| *1,5-naphthalene disulfonate* | 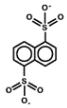 | *218 / 334* |
| *1,6-naphthalene disulfonate* |  | *224 / 337* |
| *2,6-naphthalene disulfonate* | 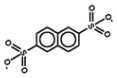 | *225 / 342* |
| *2,7-naphthalene disulfonate* | 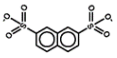 | *226 / 339* |
| *1,3,5-naphthalene trisulfonate* | 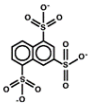 | *224 / 340* |
| *1,3,6-naphthalene trisulfonate* | 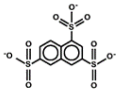 | *228 / 342* |

**Figure 1. Chemical structures and fluorescence excitation/emission wavelengths of eight naphthalene sulfonate compounds that have been widely used in geothermal reservoirs worldwide.**

In contrast to the inertness of a conservative tracer, a reactive tracer reacts in some fashion with either the rock or the solvent through processes such as thermal decay, reversible-adsorption or diffusion. With reversible adsorption, a tracer's passage through the reservoir is slightly retarded relative to that of a conservative tracer due to weakly-attractive, electrostatic forces between the tracer and the rock surface. Therefore, if a reactive tracer is co-injected and then co-produced with a conservative tracer, that relative retardation of the reversibly adsorbing tracer provides an independent variable that can serve to constrain the tracer-contacted fracture surface area (Pruess et al., 2005; Fayer et al., 2009; Reimus et al., 2012; Rose et al., 2012; Cao et al., 2020; Wu et al., 2022). And fracture surface area is important because it is directly proportional to the surface area for heat transfer and to the surface area for gas or oil production in geothermal and petroleum reservoirs, respectively.

## 2. LABORATORY EXPERIMENTS

In order to determine whether or not a candidate tracer is reversibly adsorptive, it must be subjected to controlled laboratory conditions to determine its propensity for reversible adsorption under representative reservoir conditions. We used the 2-L stainless steel reactor (Figure 2) that was fabricated by High Pressure, Inc (Erie, PA) and filled with drill cuttings from wells that were drilled into each of three Horn River shale formations (Evie, Muskwa, and Otter Park) at a Dilly Creek field site. Since the cuttings had been obtained using diesel-based drill mud, we cleaned the cuttings with solvents of increasing polarity (dichloromethane → methanol → water) in preparation for the flow experiments (Rose et al, 2012). Upon completion of the solvent-clean-up procedure, samples of the cuttings were sent to Micromeritics Analytical Services in Georgia, U.S. for surface area and porosity determination.

The reactor was designed to characterize the reversible adsorption of tracers in either cross-flow or injection/backflow mode under simulated conditions of elevated reservoir temperature and pressure. In a typical cross-flow experiment, the reactor is filled with sized drill cuttings and a solution containing the tracers is injected at one end. As the tracers are advected through the reactor, the flow of the reversibly adsorbing tracer is slowed relative to that of the conservative tracer due to its electrostatic interaction with the rock. The conservative tracer therefore exits the reactor first, followed by the reversibly adsorbing tracer. The degree of retardation is related to the reactive tracer's adsorptivity as well as the surface area of the rock within the column to which it adsorbs.

When the naphthalene sulfonates were flowed through the reactor, we observed that the flow rates of the monosubstituted naphthalenes (i.e. 1-ns and 2-ns) were slightly retarded relative to the di- and tri-sulfonated naphthalenes at the temperature (140°C) of the Dilly Creek reservoir. Furthermore, the strength of adsorption was observed to be within an appropriate range—neither too strong nor too weak—for use in this study. None of the naphthalene sulfonates—even the monosulfonated versions—had ever been observed to adsorb on geothermal reservoir rocks at any temperature.

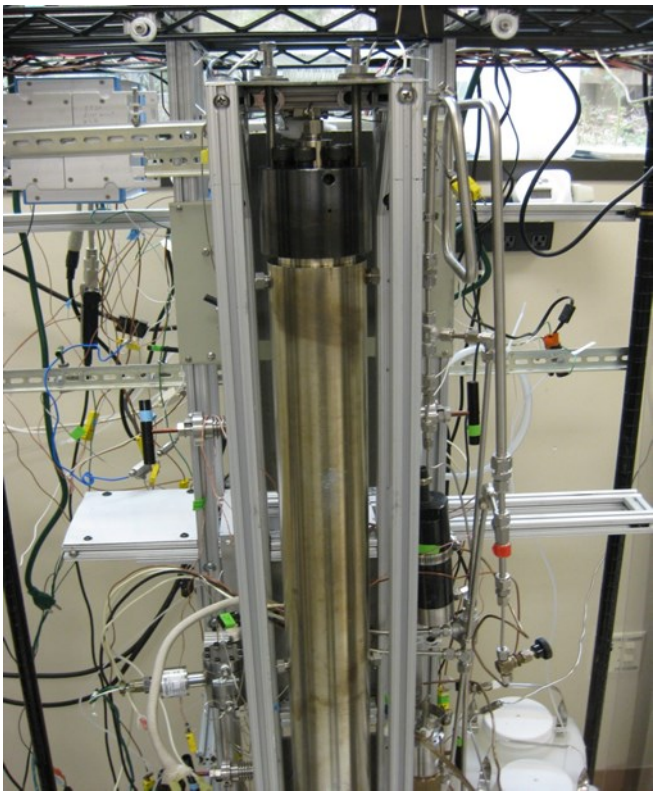

**Figure 2. Photograph of the 2-liter flow reactor with heating jacket removed to reveal the high-pressure flow cell that was filled with drill cuttings from either a Muskwa or an Evie well from the Dilly Creek, Horn River site.**

The reversible adsorption of the mono-substituted naphthalenes on shale can be explained by their chemical structures (see Figure 3). As shown by the structure of 2,6-nds on the left of the figure, the highly negative sulfonate groups are at either end of the molecule, whereas 2-ns has both a polar, sulfonated end and a neutral, aromatic end. Since the shale rocks possess a negative surface charge, the negatively charged end experiences repulsion, whereas the nonpolar—or possibly very slightly positive aromatic end—allows for a weak interaction (reversible adsorption) with the rock surface.

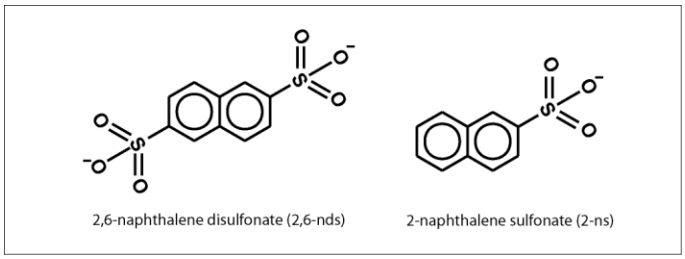


**Figure 3. 2,6-nds possesses negatively charged (polar) sulfonate groups at either end and thus behaves as a conservative tracer (like all di- and tri-sulfonated naphthalenes and halides) when flowing through Horn River shales. 2-ns possesses both a polar and a nonpolar (or very slightly positive) end and thereby behaves as a reversibly-adsorbing tracer.**

Figure 4 shows the response of a reversibly adsorbing tracer, 2-ns, and a conservative tracer, 1,5-nds, which were measured at the outlet of the reactor in crossflow mode. The reactor temperature was 140°C, its contents were alternately Evie and Muskwa cuttings, and the tracers were injected as pulses. In both cases, 1,5-nds was used as the conservative tracer and its response was the same on both rock types, whereas the flow of the 2-ns pulse was retarded relative to the conservative tracer in both the Evie or Muskwa drill cuttings—but to different extents.

When the reactor is in its injection/backflow mode, the direction of fluid flow is reversed before the injected tracer pulse reaches the reactor exit—allowing for the tracer solution to exit back through the reactor's entrance. Figure 5 plots the response of the conservative tracer 1,5-nds and the reversibly adsorbing tracer 2-ns in the injection/backflow mode. The reactor was filled with Evie drill cuttings and held at a temperature of 140 °C.

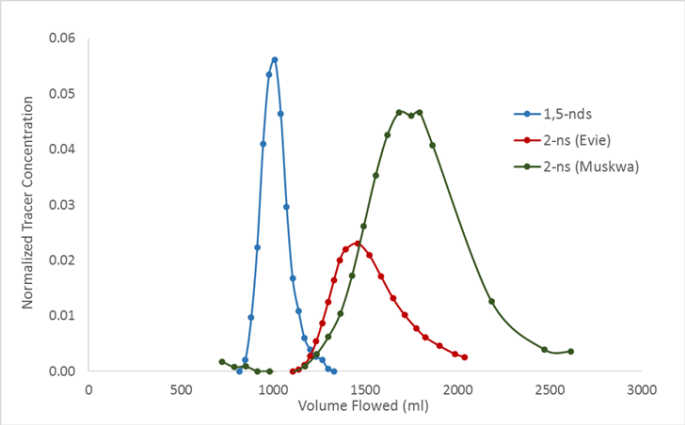


**Figure 4. Plots of a conservative tracer (1,5-nds) and a reversibly adsorbing tracer (2-ns) emerging from the 2-liter cuttings-filled reactor flowing in the cross-flow mode. The reactor was alternately filled with Evie and Muskwa cuttings and the temperature in both cases was 140°C.**

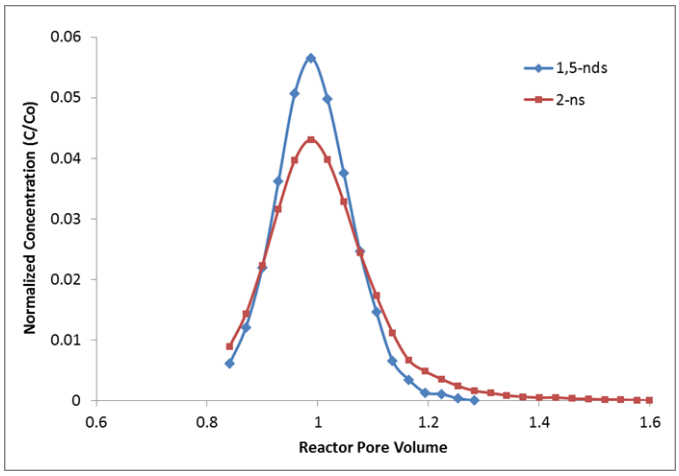


**Figure 5. Plots of a conservative tracer (1,5-nds) and a reversibly adsorbing tracer (2-ns) emerging from the 2-liter cuttings-filled reactor flowing in the injection/backflow mode. The reactor was filled with Evie drill cuttings and held at a temperature of 140°C.**

When used in the cross-flow mode, the measured tracer response can be used to quantitate a reversibly adsorbing tracer's response relative to that of a conservative tracer. This response is the relative retardation, which is related to the adsorption equilibrium constant $K_d$ by equation 1:

$$K_d = (RF - 1) * \frac{N_e}{P_b} \qquad (1)$$

where RF is the retardation factor as measured from a plot such as in Figure 4, $N_e$ is the effective porosity of the medium (pore volume divided by total column volume) and $P_b$ is the bulk density of the porous medium (mass of shale cuttings in column divided by total column volume). Table 1 shows the parameters used to measure the $K_d$'s of 2-ns on the two shale types from the laboratory column experiments.

**Table 1. Parameters Used to Determine the Kd's of 2-ns on Shales at 140°C.**

| Rock Formation | Mass of cuttings in column (gm) | Column Pore volume (ml) | Bulk Density (gm/ml) | Effective Porosity | Relative Retardation Factor | Adsorption Equilibrium Constant, $K_d$ |
|---|---|---|---|---|---|---|
| Muskwa | 3118 | 1010 | 1.454 | 0.471 | 1.60 | 0.194 |
| Evie | 2755 | 1022 | 1.294 | 0.476 | 1.51 | 0.188 |

### 3. Field Experiments

Figure 6 shows a plan view of the 10 wells (d-37-H to d-I37-H) used in the tracer testing at Dilly Creek. For simplicity, the wells are referred to by the numbers 1-10, with d-37-H being well #1 and d-I37-H being well #10. A cross-section of the 10 wells showing how they are located in the three producing formations, Muskwa, Otter Park, and Evie, is shown in Figure 7.

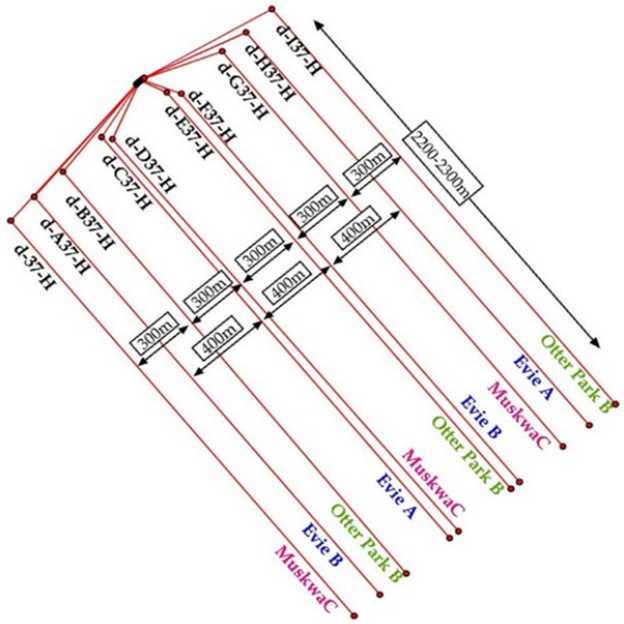


**Figure 6. Plan view of 10 study wells at the Dilly Creek site.**

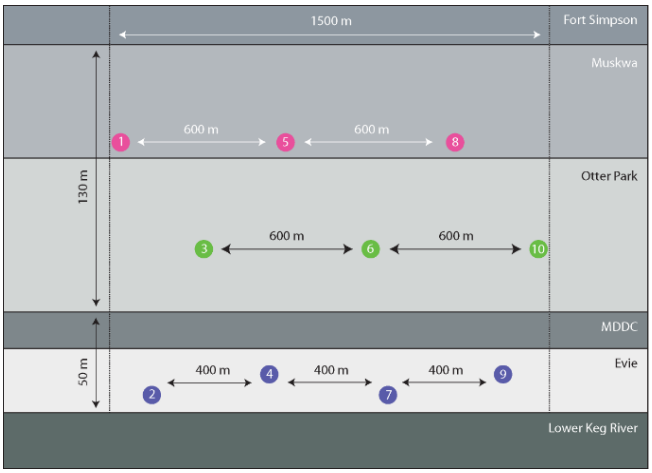


**Figure 7. Cross-section view of 10 wells at the Dilly Creek site using the same color scheme as in Figure 6.**

During the hydrofracture, a distinct combination of tracers was injected into each well according to the scheme shown in Figure 8. Into each of the 1-$m^3$ water-filled totes, the various combinations of tracers were dissolved. Then, as each stage was hydrofractured, the tracer solutions were dosed at a dilution of 1:67,000 into the hydrofracturing fluid for an initial concentration of 750 ppb for the conservative tracers and 600 ppb for the reversibly adsorbing tracer.

The intent was to inject a distinct conservative tracer (e.g. a disulfonated or trisulfonated naphthalene) and a common reversibly adsorbing tracer (i.e. 2-ns) into each of the 10 long-reach horizontal wells. Unfortunately, only six conservative tracers were available at the start of the test, so it was decided to reuse 4 of the tracers but to separate them as much as possible. The conservative tracers 1,5-naphthalene disulfonate (1,5-nds); 1,6-naphthalene disulfonate (1,6-nds); 2,6-naphthalene disulfonate (2,6-nds); 2,7-naphthalene disulfonate (2,7-nds); 1,3,5-naphthalene trisulfonate (1,3,5-nts); and 1,3,6-naphthalene trisulfonate (1,3,6-nts) were injected,

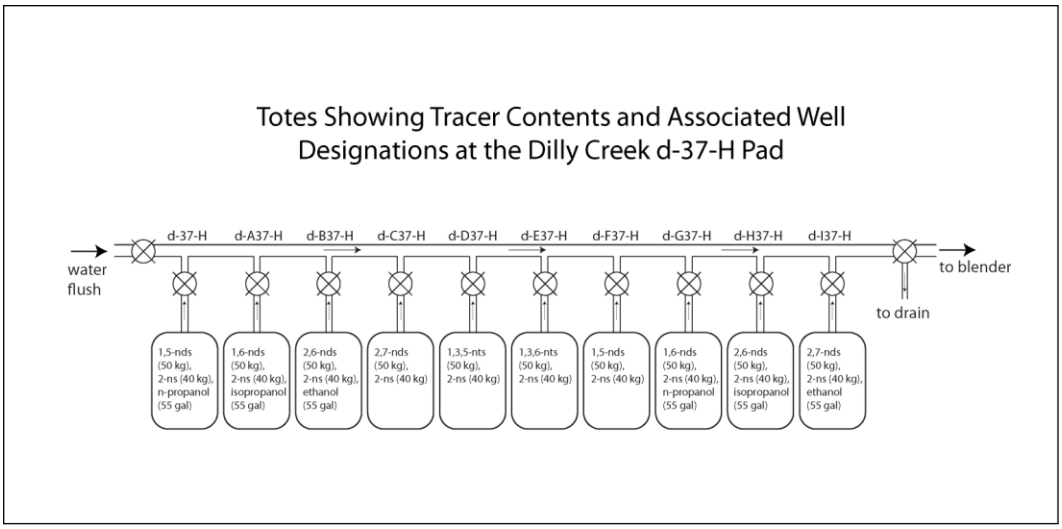


**Figure 8. A scheme showing the quantities and identities of tracers injected during the hydrofracture treatment of the 10 lon g-reach horizontal wells on the d37H wellpad. Upon flowback, the 10 wells were sampled intermittently and the samples sent to EGI for analysis.**

respectively, into wells 1-6 whereupon the pattern was repeated as the tracers 1,5-nds, 1,6-nds, 2,6-nds, and 2,7-nds were injected, respectively, into wells 7-10. Forty kg of the reversibly adsorbing tracer, 2-ns, was injected into each of the wells along with fifty kg of the conservative tracer. Although not needed for the surface-area measurement, three alcohol tracers (e.g. n-propanol, iso-propanol, and ethanol) were likewise injected into wells 1, 2, 3 and wells 8, 9, 10, respectively, in order to determine if/how two-phase (liquid and steam) flow patterns differed from liquid-phase flow patterns.

Shown in Figure 9 are the return curves of the tracers measured in well #3 according to the volume of water produced. Similar data were obtained and plotted for all 10 wells, but due to space limitations only the plot for well 3 is shown here.

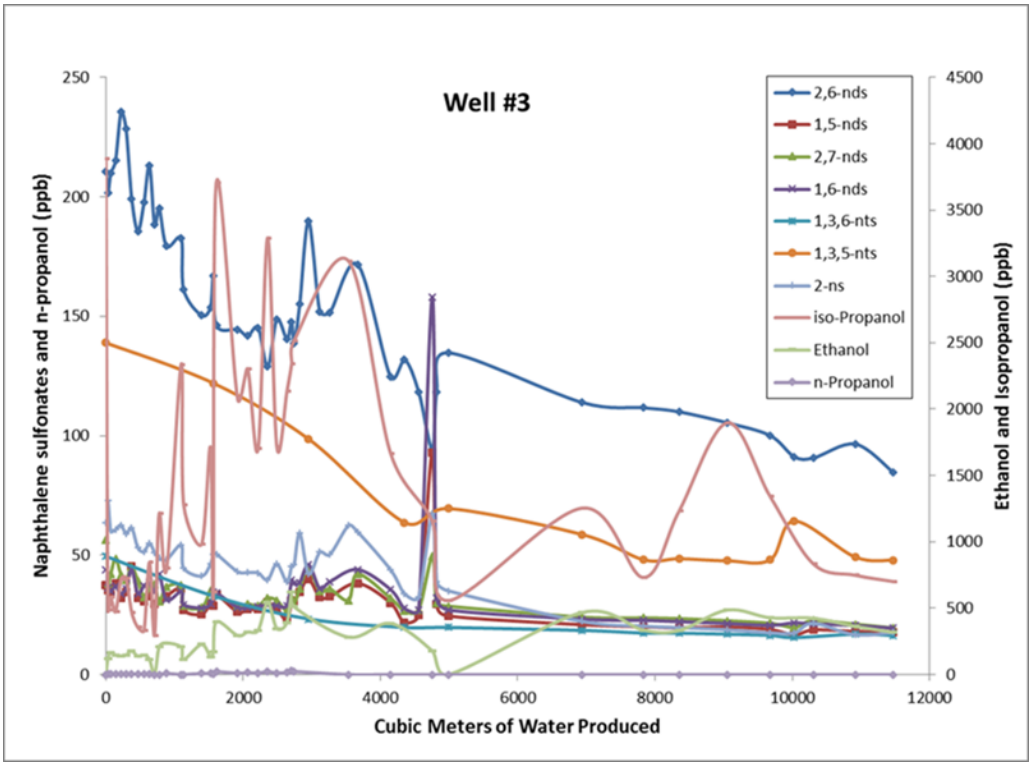


**Figure 9. Plots of tracers returned to well #3 as a function of flowback-water volume.**

One of the most important findings of this study is that within a given shale formation the adsorption of the reversibly adsorbing tracer (relative to that of the conservative tracer) increases with gas production rate. On the x axis of Figure 10 are plotted $C_{ads}/C_{con}$—the ratio

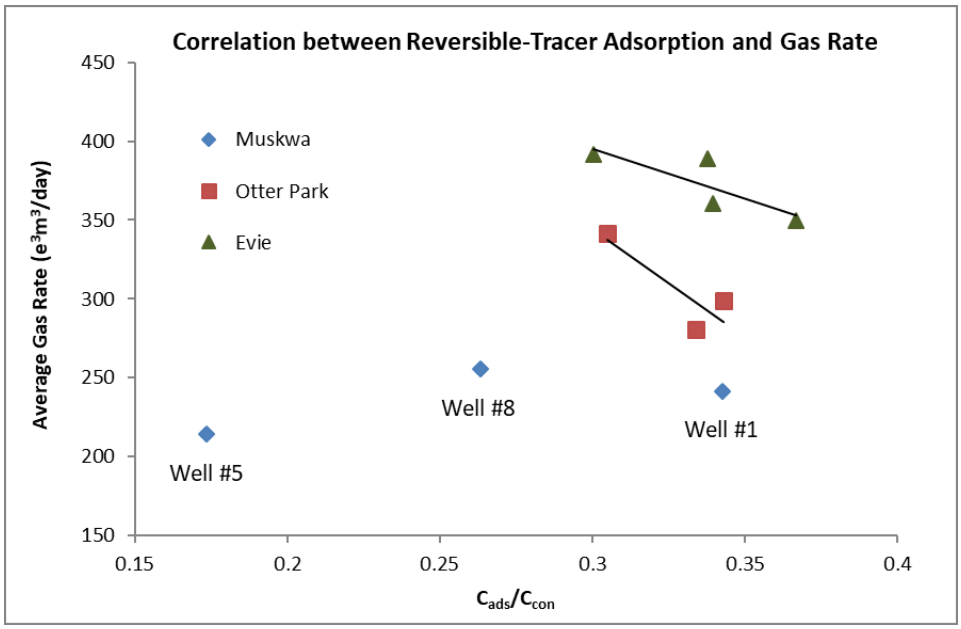


**Figure 10. A plot of reversible adsorption vs. gas production rate, showing that for the Evie and Otter Park wells the gas production rate increases as $C_{ads}/C_{con}$ decreases. A low value of $C_{ads}/C_{con}$ corresponds with high tracer adsorption.**

of the concentration of the reversibly adsorbing tracer divided by that of the conservative tracer. A low value for $C_{ads}/C_{con}$ corresponds with high adsorption and, conversely, a high value corresponds with low adsorption. As $C_{ads}/C_{con}$ increases, the reversibly adsorbing tracer is less strongly adsorbed. On the y axis of Figure 10 is plotted the average gas production rate for each well. The figure shows that tracer adsorption is correlated positively with gas productivity within a given formation—at least for the Evie and Otter Park formations. A pre-existing natural fracture connecting wells 1 and 5 in the Muskwa formation was re-opened during the hydrofracture and brine from well 5 was produced through well 1. This might explain the lack of correlation for the Muskwa wells in Figure 10.

## 4. Numerical modeling of the field experiments

### 4.1 ToughReact Grid

The ToughReact model domain is a two-dimensional cross section with a constant width (Y). The vertical (Z) direction spans the bottom of the Evie Formation to the top of the Muskwa Formation (see Figure 11). The total depth (Z) is 180 m. The central portion of the horizontal (X) direction includes the well field of 1,500 m with an additional 500 m on each side to minimize boundary condition impacts for a total horizontal length of 2,500 m.

A constant 5-m thickness (Y) and 5-m vertical element spacing (Z) was specified for the mesh. The central portion of the horizontal domain (X), which includes the well field, also had a 5-m element spacing (see Figure 11). Outside this central portion, the element spacing in the horizontal direction was progressively increased to the outer boundaries. The number of elements in the primary mesh was: 348 (X-direction) x 1 (Y-direction) x 35 (Z-Direction), yielding 12,180 total elements.

Fracture properties in the ToughReact code are built on the Tough2 code (Pruess et al. 1999) which has the Multiple Interacting Continuum (MINC) feature. MINC is an extension of the dual-porosity approach developed by Warren and Root (1963), but provides for multiple successive matrix blocks connected to the fractures. Figure 12 illustrates the MINC and fracture properties using this approach. This feature is particularly important for capturing multiple scales of matrix properties and better resolution of temperature gradients to calculate solute diffusion and heat transport into the reservoir matrix blocks. In ToughReact/Tough2, fractures are specified by defining the fracture volume, fracture porosity, and fracture spacing (Figure 13). Matrix porosity and matrix volumes are also needed for each region.

For the Dilly Creek simulations, a four-region grid partition was used, one fracture and three matrix blocks. The global flow in the domain is within the fracture partition. The matrix blocks are connected to the fractures, but not to each other (i.e. matrix blocks are bounded by fractures). Matrix blocks were subdivided into three regions (M1, M2, and M3) so that the final ToughReact mesh has four times the number of elements as the base mesh (48,720 elements).

A grid spacing test was run using a 3-m horizontal element spacing in the central portion of the domain. This mesh only had 1 matrix region yielding a total of 38,920 elements. The results of this test case were similar to the 5-m horizontal grid spacing with one matrix region, therefore the 5-m mesh was used for computational efficiency.

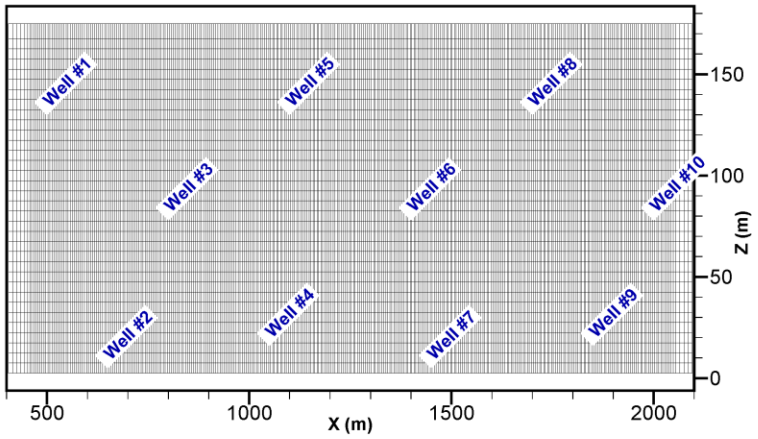


**Figure 11. The central portion of the ToughReact mesh with 5-m X-Z spacing with a 5-m Y-direction thickness. Entire domain extends from 0 to 2500 m. Note: Vertical Exaggeration is 5X.**

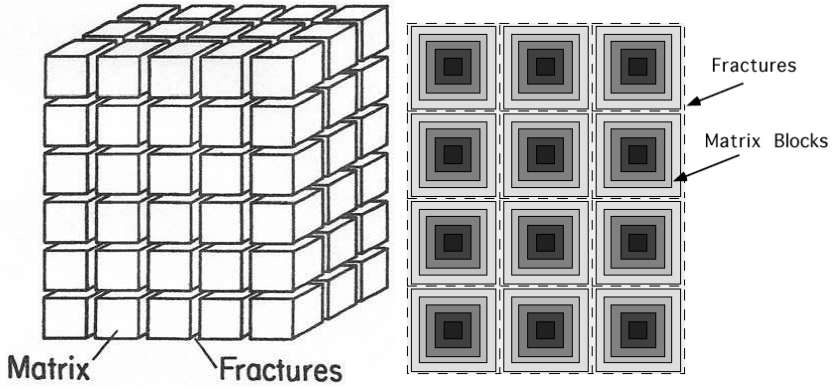


**Figure 12. Dual Porosity Model (Warren and Root, 1963) and ToughReact MINC subgridding with fractures. From Pruess 1983; Pruess 1992; Pruess, Oldenburg, and Moridis, 1999.**

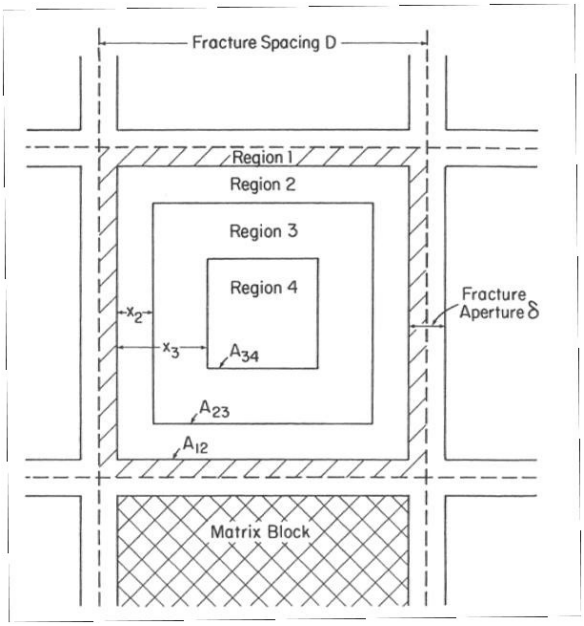


**Figure 13. MINC partitioning of an idealized fracture system (Pruess, Oldenburg, and Moridis, 1999; Pruess, 1983)**

### 4.2 Properties

Two material types were specified in the model: Matrix and Fracture. Initial properties (porosity, permeability, etc) were set to nominal values. Porosities were fitting parameters as part of this analysis. The fitted porosities for the matrix do not represent the total shale porosities or effective porosities, but represent the mobile, fluid-saturated portion of the matrix that is available to interact with the tracers.

Kd's for the reversibly-adsorbing tracer (2-ns) were set based on results of laboratory experiments of cuttings from the Muskwa and the Evie shales conducted at reservoir conditions (see Table 1). The Evie shale values were also used for the Otter Park Formation and MDDC.

The tracer diffusion coefficient used in these simulations was based on a 25 °C measurement for 2-ns (Hatsuho Uedaira and Hisashi Uedaira, 1963) of 9.8E-10 $m^2/s$. It is expected that the diffusion coefficients would be much higher at reservoir conditions at 140 °C. However, ToughReact does not have a separate hydraulic dispersion coefficient and includes numerical dispersion based on the 5-m grid spacing. The ToughReact diffusion coefficient should be viewed as a combination diffusion and dispersion coefficient. While different values have not been rigorously tested, a constant value approximately 3 times the 25 °C value was selected based on comparison of simulated tracer concentrations vs. field measurements for some cases. Sensitivity cases over a range of diffusion coefficients should be conducted in future work to see the impact on the results.

### 4.3 Initial Conditions

Fluid Pressures in the domain were arbitrarily set to 6.895E+06 Pa and a temperature of 140 °C. A pseudo steady state run was then conducted to achieve hydrostatic pressures. Initial tracer concentrations were set to zero.

### 4.4 Boundary Conditions

The top and bottom of the domain were set to no-flow boundaries due to the low permeability of Fort Simpson Formation above the reservoir and the Lower Keg River below the reservoir. The front and back of the 5-m length of the domain were also set to no-flow boundary conditions because of the symmetry of the reduced length grid. The fluid pressures on side boundaries (Z-direction) of the domain are held (Dirichlet) at the values calculated by the results of the steady state run (i.e. hydrostatic conditions).

### 4.5 Operational Setup

Operational information from the test was analyzed to develop the timing and rates for the simulation. Since the simulated domain is only a portion of the field site, an operation in the middle of the injection period was used to determine the injection timing and shut-in period. Flow rates and tracer masses were scaled to the simulated 5-m well length (see Tables 2 and 3). The simulated injection flow rate and duration was the same for all wells based on the analyses of the operational duration. However, flowback rates were different for each well (Table 3) because of the large range in recovery volumes during that period. As described in Section 3, 50 kg of a conservative tracer was injected into each well along with 40 kg of reversibly-adsorbing tracer (2-ns).

The injection of each well was conducted in a separate simulation run since excessive hydraulic interference of the tracer plumes was occurring during that simulation period. However, production was simultaneously simulated from all wells during the flowback period.

**Table 2. Field Test Operational Details used in the Simulations.**

| | Operational Duration | Operational Flow Rates | Simulation Duration | Simulation Flow Rates |
|---|---|---|---|---|
| **Injection 2013/7/05 to 2013/8/11 (36 days)** | Mean Values per Frac Stage:<br>Duration: 3 hrs.<br>Well Length: 87.25 m.<br>Fluid Volume: 2460 $m^3$ | 13.7 $m^3$/min for 180 min | 24 hours (extended due to simulation convergence at high flow rates) | Scaled rate to 5-m well length (grid width):<br>140.5 $m^3$ / 24 hrs = 0.0967 $m^3$/min |
| **Shut-in** | Mean: 59 Days | NA | 76 Days (midpoint of injection plus shut-in) | NA |
| **Flowback** | 90 Days (mean) | Variable | 90 days | Different for each well based on recovery volume (see Table 3) |

**Table 3. Flowback Volumes for Each Well.**

| Well Designation | Flowback Volume ($m^3$) | Duration (days) | Average Flow Rate for 90 days ($m^3$/day) | Scaled Simulation Production Rate (5-m width) ($m^3$/day) |
|---|---|---|---|---|
| Well 1 | 16,311.2 | 101.6 | 181.24 | 0.4027 |
| Well 2 | 6,945.4 | 83.6 | 77.17 | 0.1715 |
| Well 3 | 11,462.6 | 92.4 | 127.36 | 0.2830 |
| Well 4 | 9,694.7 | 77.6 | 107.72 | 0.2394 |
| Well 5 | 18,959.9 | 97.6 | 210.67 | 0.4681 |
| Well 6 | 11,479.2 | 97.0 | 127.55 | 0.2834 |
| Well 7 | 6,595.4 | 82.1 | 73.28 | 0.1628 |
| Well 8 | 17,319.0 | 99.0 | 192.43 | 0.4276 |
| Well 9 | 3,978.1 | 81.5 | 44.20 | 0.0982 |
| Well 10 | 10,326.5 | 77.2 | 114.74 | 0.2550 |

### 4.6 Simulation Results

An iterative process was used to analyze/fit the field test results. First, simulations are configured based on the operational data from the test (injection concentrations, rates and times; shut-in period; flowback rates and times, including any flow stoppages). The initial simulation configuration also includes implementation of the laboratory-derived reactive tracer transport properties (if available) at the reservoir conditions (e.g., sorption, reaction networks, thermal degradation, diffusivities). Then the conservative tracer concentration histories are fit by adjusting flow and transport properties (diffusion, porosities, and matrix volumes). Next, reactive tracer concentration histories are fit by adjusting the fracture volume, porosity, and fracture spacing. The reactive tracer data fit may also require adjustments to the transport properties, specifically the matrix volumes and porosity. Because the properties interact, this process is repeated iteratively to obtain the best fit for both types of tracers. Cumulative tracer mass recovery is also an important consideration during the fitting process, particularly if the concentration data are noisy.

The best-fit case for each well was obtained from a series of runs with varying parameters based on overall fit the conservative and reversibly-adsorbing tracer. Early times for the conservative tracer were not given much weight due to potential excessive numerical dispersion from the 5-m grid spacing and the sensitivity of the conservative tracer to heterogeneities (compared to the reversibly-adsorbing tracer). In addition to the concentration comparison, the total mass returns were also considered for selection of the final cases.

Figure 14 shows a comparison of the simulated results with the field data for well 3. Similar plots for the remaining nine wells are shown in the full report (Rose et al., 2015), but, for brevity, not repeated here.

The final parameters used for each well are listed in Table 4. The simulated volumes and masses in these plots are scaled to the full well length. Solid lines in these figures are the measured and simulated conservative and reversibly-adsorbing tracer concentrations on the primary Y axis. The dashed lines are the measured and simulated cumulative mass recovery for each tracer on the secondary Y axis. In addition to the tracer concentrations, the fit of the cumulative mass recovery was also considered.

Overall the fits for the simulated vs. measured reversibly-adsorbing tracer were good. As mentioned previously, the overall fits do not capture the initial high conservative tracer concentrations that were measured in some wells. This is likely due to the conservative tracer being more sensitive to high permeability layers or heterogeneities than the reversibly-adsorbing tracer. The late time data should also be given more weight since only small fractions of the fluid and tracer were recovered during the flowback. The simulated total mass recoveries were also close to the values calculated from the measurements, but in some cases the simulated concentrations were low at the beginning and higher at the end. For fitting tracer data for each well, the mass recovery data for tracers in the other wells was not explicitly used (see Section 3.4). Those data should be considered in future work.

The availability of additional site data would have helped constrain the model (e.g. geologic logs, wireline logs, core analysis, and geophysical measurements). The simplistic geologic model developed in this study could be refined and results constrained if these types of data become available.

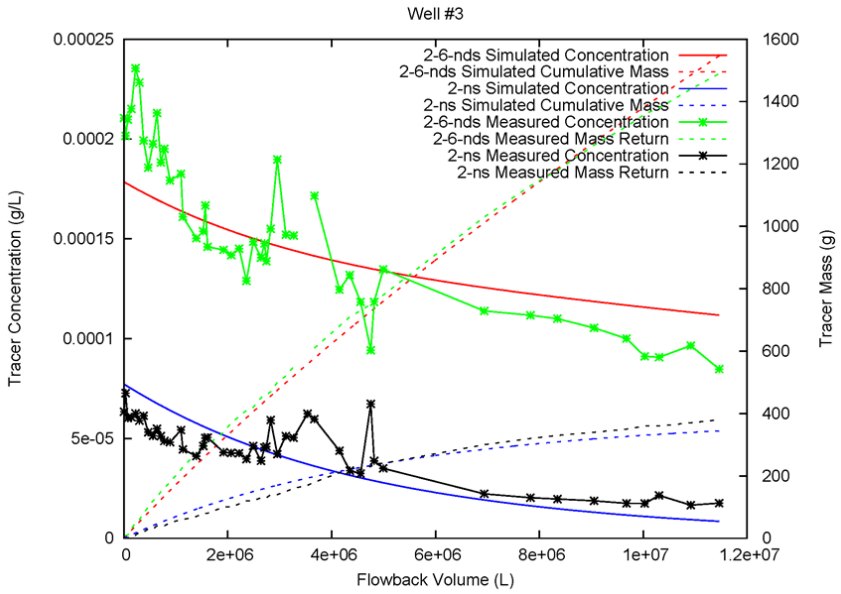


**Figure 14. Well 3 (Otter Park Formation) simulation fit.**

**Table 4. Properties used for fitting wells. M2 Region = 0.3 and M3 Region is the remaining volume fraction. Fracture Surface Area per unit Reservoir Volume is calculated from specified Fracture Spacing (see Figure 12).**

| Well | Formation | Matrix Porosity | M1 Region | Facture Volume | Fracture Spacing (m) | Fracture Surface Area Per Unit Reservoir Volume ($m^2/m^3$) |
|---|---|---|---|---|---|---|
| **3** | Otter Park | 0.015 | 0.27 | 0.0008 | 3.20 | 1.8735 |
| **6** | Otter Park | 0.015 | 0.25 | 0.0008 | 3.40 | 1.7633 |
| **10** | Otter Park | 0.015 | 0.27 | 0.0008 | 3.20 | 1.8735 |
| **2** | Evie (lower) | 0.015 | 0.20 | 0.0008 | 4.00 | 1.4988 |
| **4** | Evie (upper) | 0.015 | 0.27 | 0.0008 | 3.50 | 1.7129 |
| **7** | Evie (lower) | 0.015 | 0.23 | 0.0008 | 4.00 | 1.4988 |
| **9** | Evie (upper) | 0.015 | 0.24 | 0.0008 | 3.90 | 1.5372 |
| **5** | Muskwa | 0.015 | 0.25 | 0.0008 | 3.10 | 1.9339 |
| **8** | Muskwa | 0.015 | 0.25 | 0.0008 | 3.25 | 1.8447 |

Processes and features not included in this modeling study are:

- Differences in material properties between main units (e.g. porosity, grain density, permeability) except for Kds in Muskwa and Evie formations (data limitation).
- Heterogeneities / sub-layering within each unit (data limitation)
- Imbibition / Drainage of dry shales (assumed water saturated)
- Tracer Interaction with Fracking Fluid

Figure 15 shows a comparison between the simulated fracture surface area and the average gas production rate for the nine wells that were included in the numerical simulation. The plot indicates that as the fracture surface area increases the average gas production rate decreases. This is counterintuitive to what might be expected from the results plotted in Figure 10, which shows that—within each formation—the relative degree of tracer reversible-adsorption increases (more adsorption makes the ratio of the slope of $C_{ads}$ to the

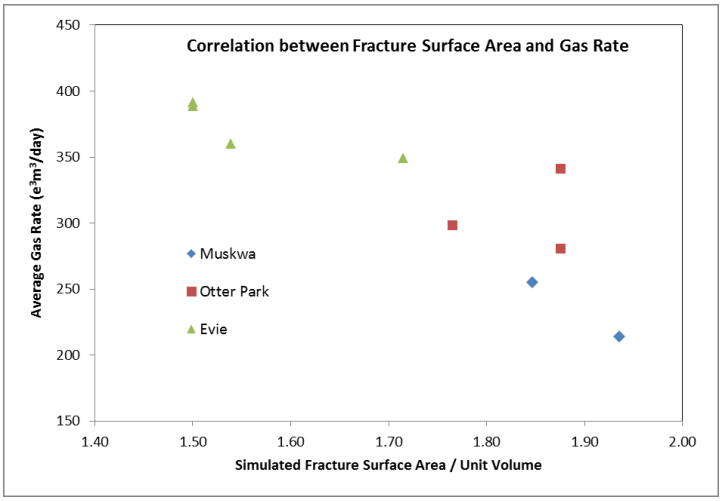


**Figure 15. Comparison of fracture surface area derived from model fits to average gas production rates.**

slope of $C_{con}$ decrease) as the gas production rate increases. This apparent contradiction can be explained by the fact that the numerical simulation accounts for the surface area of the fractures only and does not include the surface area within the pores. As shown in the appendices (Rose et al., 2015), the BET surface areas are 11.0 $m^2/g$, 16.0 $m^2/g$ and 17.4 $m^2/g$ for the Muskwa, Evie and Otter Park cuttings, respectively. Thus, the overall-rock surface area, which is the area with which the reversibly adsorbing tracer reacts, is much larger than the relatively small surface of the fractures themselves, which is the fracture-surface area used in the model.

## SUMMARY AND CONCLUSIONS

Using a laboratory flow reactor filled with drill cuttings, we studied the behavior of several candidate tracers under conditions that simulated a shale-gas reservoir in British Columbia, Canada. The naphthalene sulfonate and short-chain-aliphatic alcohol tracers had already been qualified for use as geothermal tracers, but never before for broad use in a shale-gas hydrofracture experiment. All of the di- and tri-sulfonated tracers were all observed to behave conservatively in the laboratory experiments, whereas the mono-sulfonated naphthalene, 2-naphthalene sulfonate, was observed to adsorb reversibly.

Based on the results of the laboratory experiments, a distinct naphthalene sulfonate tracer was injected into each of 10 long-reach horizontal wells during their hydrofracture at the field site. Upon flow-back, the concentrations of the conservative and reversibly adsorbing tracers were measured in the produced brine solutions. Plots of tracer adsorption vs. gas-production rates showed a positive correlation between the two, at least for two of the three formations studied.

A numerical flow model was constructed in order to correlate flowback-gas production with reactive-tracer adsorption. The model showed an inverse correlation between fracture surface area and gas production rate. This apparent contradiction might be explained by the fact that the numerical simulation accounts for the surface area of the fractures only and does not include the surface area within the pores. Likewise, neither the conceptual model nor the numerical simulation model accounts for the reopening of naturally occurring fractures during the hydrofracture process.

This study shows the power of the use of reversibly adsorbing tracers in combination with conservative tracers for predicting the performance of hydrofractured wells in an unconventional-petroleum field at geothermal-reservoir temperatures.

## References

Cao S., Schaffer, M., Taherdangkoo, R., and Licha, T. (2020) Solute reactive tracers for hydrogeological applications: A short review and future prospects, *Water*, MDPI, Basel, Switzerland.

Fayer S., P. Rose, S. Petty, M.D. Deo, and T. Xu. (2009), A Computational Technique for Estimating the Fracture Surface Area Adjacent to a Newly Stimulated Well within an Engineered Geothermal System. Proceeding Tough Symposium September 14-16, 2009. Lawrence Berkeley Laboratory. Berkeley, CA.

Greim, H.; Ahlers, J.; Bias, R.; Broecker, B.; Hollander, H.; Gelbke, H.-P.; Klimisch, H.-J.; Mangelsdorf, I.;Paetz, A.; Schön, N.; et al. Toxicity and ecotoxicity of sulfonic acids: Structure-activity relationship *Chemosphere*, **1994**, 28, 2203–2236.

Pruess, K., van Heel, T., and Shan, C. (2005) Tracer Testing for Estimating Heat Transfer Area in Fractured Reservoirs, Pr*oceedings World Geothermal Congress 2005*, Antalya, Turkey, 24-29 April 2005.

Reimus, P. Williams, M., Vermeul, V., Rose, P.E., Leecaster, K., Ayling, B. Sanjuan, R., Ames, M., Dean, C., and Benoit, R.M. (2012) Use of Tracers to Interrogate Fracture Surface Area in Single-Well Tracer Tests in EGS Systems, *Proceedings, 37th Workshop on Geothermal Reservoir Engineering*, Stanford University SGP-TR-194.

Rose, P.E., Benoit, W.R., and Kilbourn, P.M., (2001), The application of the polyaromatic sulfonates as tracers in geothermal reservoirs: *Geothermics*, 30(6), pp. 617-640.

Rose, P.E., Capuno, V., Peh, A., Kilbourn, P.M., and Kasteler, C. (2002a) The Use of the Naphthalene Sulfonates as Tracers in High Temperature Geothermal Systems, *Proceedings 23rd PNOC Geothermal Conference.*

Rose, P.E., Johnson, S.D., and Kilbourn, P.M., and Kasteler, C. (2002b) Tracer Testing at Dixie Valley, Nevada Using 1-Naphthalene Sulfonate and 2,6-Naphthalene Disulfonate: *Proc. Twenty-Seventh Workshop on Geothermal Reservoir Engineering*, Stanford University, SGP-TR-171.

Rose, P.E., Mella, M., and Kasteler, C., (2003) A new tracer (1,3,5-naphthalene trisulfonate) for use in liquid-dominated, high-temperature geothermal reservoirs: GRC Transactions, 27, pp. 403-406.

Rose, P.E., Mella, M., Kasteler, C., and S.D. Johnson, (2004) The Estimation of Reservoir Pore Data from Tracer Data: *Proceedings, 29th Workshop on Geothermal Reservoir Engineering*, Stanford University SGP-TR-175.

Rose, P.E., Leecaster, K., Clausen, S., Sanjuan, R., Ames, M., Reimus, P., Williams, M., Vermeul, V., and Benoit, R. (2012) A Tracer Test at the Soda Lake, Nevada Geothermal Field Using a Sorbing Tracer, *Proceedings, 37th Workshop on Geothermal Reservoir Engineering*, Stanford University SGP-TR-194.

Rose, P.E., Oates, J. and Williams, M. (2015) "Tracer Testing to Characterize Flow Processes Resulting from the Hydrofracture of a Horn River Shale Reservoir", Final Report to Nexen Energy ULC, Calgary, Alberta.

Sajkowski, L. (2020) "The thermal stability of the naphthalene sulfonic acids under geothermal conditions", Ph.D. dissertation, Victoria University of Wellington; Wellington, New Zealand.

Shook, G.M., and Forsman, J.H. (2005) "Tracer Interpretation Using Temporal Moments on a Spreadsheet", INL Report INL/EXT-05-00400.

Wu, H., Fu, P., Hawkins, A.J., Tang, H., and Morris, J.P. (2022) "Predicting thermal performance of an enhanced geothermal system from tracer tests in a data assimilation framework", *Water Resources Research*, in press.